Computer Science Department of The University of Auckland
CITR at Tamaki Campus (http://www.citr.auckland.ac.nz)

CITR-TR-94 August 2001

Analysis of Symmetric Panorama Acquisition

Shou Kang Wei, Fay Huang, and Reinhard Klette[1]

Abstract

This paper reports about basic algebraic relations between parameters and an error analysis for symmetric panorama acquisition. Symmetric panoramas are of importance in computer vision, computer graphics, and stereoscopic imaging and display. Advantages of symmetric panoramas include the possible reuse of stereo matching algorithms previously developed for 3D reconstruction, and possible applications in stereoscopic visualization. This paper formulates and studies problems which have not yet been approached previously: algebraic relations between application-specific parameters and imaging parameters, and how errors (incurred from measurements during imaging) are propagating and impacting the quality of resultant images. Without dealing with such problems, we are not able to answer the more difficult questions regarding the design and/or the capability assessment of symmetric panorama acquisition systems. The paper first summarizes the acquisition geometry followed by in-depth studies of algebraic parameter relations and error analyses.

[1] Center for Image Technology and Robotics Tamaki Campus, The University of Auckland, Auckland, New Zealand. shoukang, fay, r.klette@auckland.ac.nz

Analysis of Symmetric Panorama Acquisition

Shou Kang Wei, Fay Huang and Reinhard Klette

CITR, Computer Science Department, The University of Auckland
Tamaki Campus, Auckland, New Zealand

Abstract

This paper reports about basic algebraic relations between parameters and an error analysis for symmetric panorama acquisition. Symmetric panoramas are of importance in computer vision, computer graphics, and stereoscopic imaging and display. Advantages of symmetric panoramas include the possible reuse of stereo-matching algorithms previously developed for 3D reconstruction, and possible applications in stereoscopic visualization. This paper formulates and studies problems which have not yet been approached previously: algebraic relations between application-specific parameters and imaging parameters, and how errors (incurred from measurements during imaging) are propagating and impacting the quality of resultant images. Without dealing with such problems, we are not able to answer the more difficult questions regarding the design and/or the capability assessment of symmetric panorama acquisition systems. The paper first summarizes the acquisition geometry followed by in-depth studies of algebraic parameter relations and error analyses.

Keywords: panorama acquisition, symmetric panoramas, imaging parameters.

1 Introduction

Panoramic imaging receives increasingly interest in the communities of computer vision and computer graphics. In particular, stereoscopic panoramas providing 3D scene information are of great interest for stereo visualization and shape reconstruction. Among possible stereoscopic panoramas [WHK00], the symmetric panorama (see Sec. 2 for details) allows stereoscopic-viewable images and supports the reuse of stereo-matching algorithms, previously developed for 'traditional' binocular stereo images.

The basic purpose of a stereoscopic panorama imaging system is being capable to acquire 3D scenes of interest (1) in desired pictorial compositions and (2) having a sufficient diversity in depth levels (disparities) demanded by the application. Design principles of a panoramic imaging system have to pay attention to: (1) the relevant variation of 3D scenes of interest; (2) a desirable flexibility in adjustments of camera-to-scene distances and the availability of different angles of lenses with respect to differing demands for fields of view; (3) the desired controllability of possible depth levels for the intentioned application (e.g. defined by the screen resolution in case of stereoscopic visualization).

These aspects result into design-questions/issues which need to be answered/considered in order of building a stereoscopic panorama imaging system. Given is a family of 3D scenes of interest, an interval of possible distances between camera and closest scene objects, and a scale of depth levels demanded in the application. What should be the value of the radius R of the focal circle and what are the relevant intervals for projection angles ω (see Sec. 2 for the definitions) of a stereoscopic panorama imaging system? On the other hand, since the radius of the focal circle and the interval of projection angles are limited due to physical/cost constraints, given the realizable/available radius and angle intervals, what is the family of 3D scenes, the interval of camera-to-scene distances and the scale of depth levels of a system following these constraints? Furthermore, what are possible errors which can affect the result (scene decomposition and depth levels) using the designed system, and by how much these errors can affect the result?

To answer questions like these, basic relations between application requirements, image acquisition models, and specifications of given families of 3D scenes need to be understood. Unfortunately, the analysis of such relations is not yet discussed in the literature on panoramic imaging. Previous studies pay great attention on how the proposed imaging approach could support a chosen area of application [IYT92, Che95, SS97, WHK99, PBE99, SKS99, SH99, Sei01]. This paper discusses basic relations and error analysis for symmetric panoramic imaging.

The paper is organized as follows. Section 2 briefly reviews the acquisition geometry and supporting models for analysis. Section 3 discusses the analysis of basic relations and interprets the obtained results geometrically. Section 4 performs error analysis and demonstrates the results for typical image acquisition situations. Conclusions and orientations for future work are given at the end of the paper.

2 Acquisition Geometry

The conceptual model and an implementation of stereoscopic panoramic image acquisition (using a line camera) is depicted in Fig. 1(A) and (B). Fundamental geometric studies for this model are reported in [HWK01]. The focal point $\mathbf{C}$ of a slit camera [RS97] is rotated with respect to a rotation center $\mathbf{O}$. The optical axis must pass through both $\mathbf{O}$ and $\mathbf{C}$. The effective focal length, denoted as f, and the CCD element size (or pixel size), denoted as u, are assumed to be given.

The circle describing the path of all focal points during rotation is called *focal circle*. The distance between the slit camera's focal point and the rotation axis, denoted as R, remains constant for a stereoscopic panorama imaging process. The angular interval of every subsequent rotation step is assumed to be constant.

Each slit image contributes one column to a panoramic image of dimension $W_P \times H_P$ (in pixels). An angle ω is defined by the angle between the normal vector of the focal circle at the associated focal point, and the optical axis of the slit camera. A panoramic pair of ω and $(360^\circ - \omega)$ is referred to as a *symmetric pair*. The epipolar geometry of such a symmetric pair is characterized by epipolar lines being image rows [HWK01]. This paper focuses on this symmetric case.

We consider two main demands for image acquisitions: first, allow proper *scene composition* (coverage of important scene features, sufficient representation of geometric complexity etc.) in resultant images, and second, allow desirable depth levels (or spatial disparities) over a family

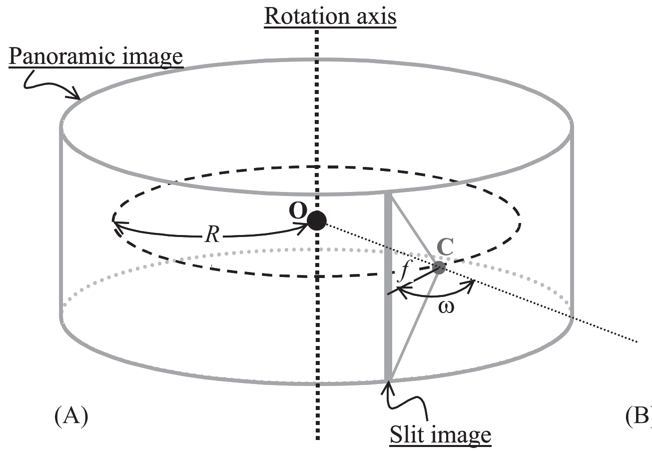

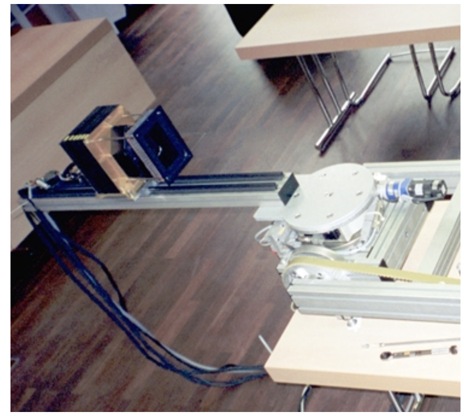

Figure 1: (A) The stereoscopic panoramic imaging model. See text for details. (B) Stereoscopic panorama camera at the space sensory institute of DLR (German Aerospace Center).

of scenes of interest in the resultant images. The analysis of algebraic relations, ensuring that requirements can be met, requires a definition of a mathematical model and a precise specification of parameters involved.

Region of Interest: We propose a simple model consisting of two concentric cylinders, where the smaller one has radius D_1 and the larger one has radius D_2, with $D_1 < D_2$. The space between both cylinders contains the region of interest (*RoI*), which is also limited in height due to the distance between camera and RoIs described below. Accurate distance values or stereo visualizations are desirable for the RoI.

Distance of Camera to RoI: In order to compose a scene within the RoI properly into resultant images, the distance between **C** and points on the smaller cylinder needs to be estimated. (ideally, it should be constant for a 360° panorama acquisition, but this might be in conflict with further constraints). We denote the distance as H_1. The valid interval of H_1 is lower-bounded by the minimum focusable distance, and it is $H_1 < 2 \times D_1$ because the camera is assumed to be inside of the smaller cylinder.

Resolution: Since the resolution W_P limits the possible depth level/disparity in the resultant stereoscopic images, we assume $W_P > d_r$, where d_r is the possible disparity maximum in an application. The formula for computing W_P of a 360° panorama is as follows,

$$W_P = \frac{2\pi f}{u} \frac{D_1}{H_1}. \tag{1}$$

Depth Level, Disparity, and Angular Disparity: *Angular disparity* is defined by the angle between two rays, starting at **O** and passing through a pair of corresponding projections of a 3D point. A 3D point defines two angular disparities on cylinders of radius D_1 or D_2 and these are denoted as θ_1 and θ_2. The *width of the angular disparity interval* (for one 3D scene point) is equal to $\theta_r = \theta_2 - \theta_1$. Spatial ('normal') disparities in image space are denoted as d_1 and d_2, corresponding to θ_1 and θ_2. Similarly, $d_r = d_2 - d_1$ is the *width of the disparity interval.* Note that all d_r values are measured along image rows for a symmetric pair. The conversion between θ_r and

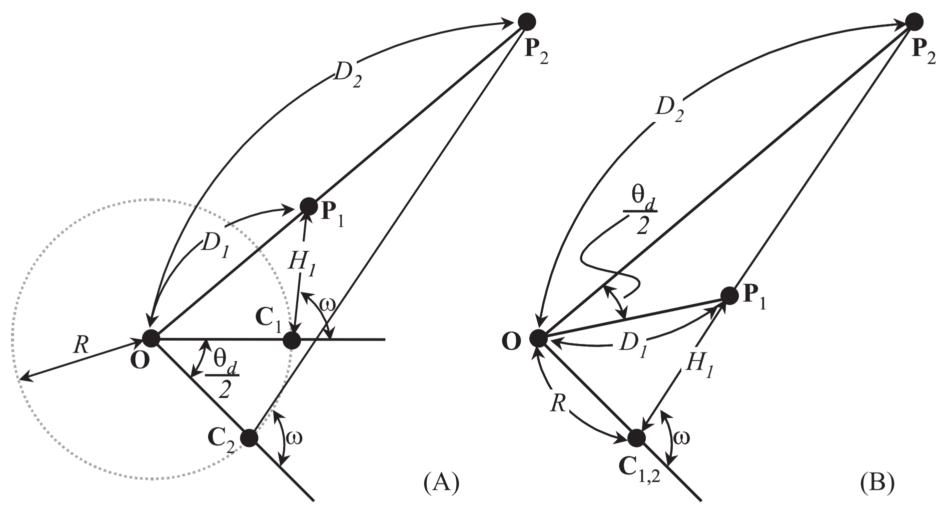

Figure 2: The acquisition geometry of symmetric panoramas, (A) and (B) are before and after the transformation defined in the text.

d_r is

$$\theta_r = \frac{2\pi d_r}{W_P}. \tag{2}$$

The potential intervals of θ_r and d_r are $0° < \theta_r < 180°$ and $0 < d_r < \frac{W_P}{2}$.

The acquisition geometry of symmetric panoramas is shown in Fig. 2. The two triangles $\triangle \mathbf{OP}_1\mathbf{C}_1$ and $\triangle \mathbf{OP}_2\mathbf{C}_2$ in Fig. 2(A) can be transformed such that the point $\mathbf{C}_1$ coincides with the point $\mathbf{C}_2$ (i.e. a rotation transformation of θ_r degrees with respect to $\mathbf{O}$). The geometry of these two triangles after the transformation is depicted in Fig. 2(B).

3 Analysis of Parameter Relations

From Fig. 2(B), R and ω can be found in terms of D_1, D_2, H_1 and θ_r. We have

$$R = \sqrt{D_1^2 + H_1^2 + 2D_1H_1 \frac{D_1 - D_2\cos\theta_r}{\sqrt{D_1^2 + D_2^2 - 2D_1D_2\cos\theta_r}}}, \tag{3}$$

and

$$\omega = \arccos\left(\frac{D_1D_2\cos\theta_r - D_1^2 - H_1\sqrt{A}}{\sqrt{A(D_1^2 + H_1^2) + 2D_1H_1(D_1 - D_2\cos\theta_r)\sqrt{A}}}\right), \tag{4}$$

where $A = (D_1^2 + D_2^2 - 2D_1D_2\cos\theta_r)$.

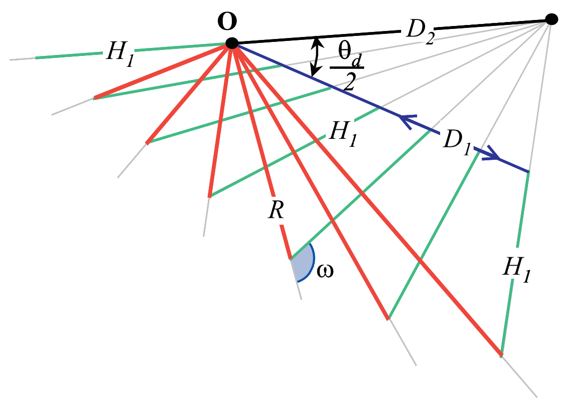

Figure 3: The geometry of the changes in D_1 values and related changes in R and ω.

If one of the values D_1, D_2, H_1 and θ_r varies and the other three are kept constant, both the values of R and ω vary correspondingly. In this section, we study how the change of each of D_1, D_2, H_1 and θ_r affects the change of each of R and ω.

3.1 How does the change of D_1 affect R and ω?

The value of D_1 is defined to be in the interval between 0 and D_2 exclusively. The geometry of changing D_1 values versus changes in R and ω values is depicted in Fig. 3.

When D_1 goes to one of the two extreme values 0 or D_2, the values of R are denoted as R_- and R_+ respectively. These can be written in limit notation as follows:

$$\lim_{D_1 \to 0^+} R = R_-, \text{ and } \lim_{D_1 \to D_2^-} R = R_+.$$

Using Eq. 3, it can easily be shown that $R_- = H_1$, and the value of R_+ is as follows:

$$R_+ = \sqrt{D_2^2 + H_1^2 + 2D_2H_1 \sin\left(\frac{\theta_r}{2}\right)}. \tag{5}$$

Similarly for ω, we write

$$\lim_{D_1 \to 0^+} \omega = \omega_-, \text{ and } \lim_{D_1 \to D_2^-} \omega = \omega_+.$$

From Eq. 4, it can easily be shown that $\omega_- = 180°$, and the value of ω_+ is as follows:

$$\omega_+ = \arccos\left(\frac{-H_1 - D_2 \sin\left(\frac{\theta_r}{2}\right)}{\sqrt{D_2^2 + H_1^2 + 2D_2H_1 \sin\left(\frac{\theta_r}{2}\right)}}\right).$$

From Eq. 5 we know that $R_+ > H_1$, i.e. $R_+ > R_-$. Moreover, from Fig. 3, we may observe that R_+ is the upper bound of R for all values of D_1 in the interval $(0, D_2)$. In other words, the value of R reaches its maximum when D_1 goes to D_2.

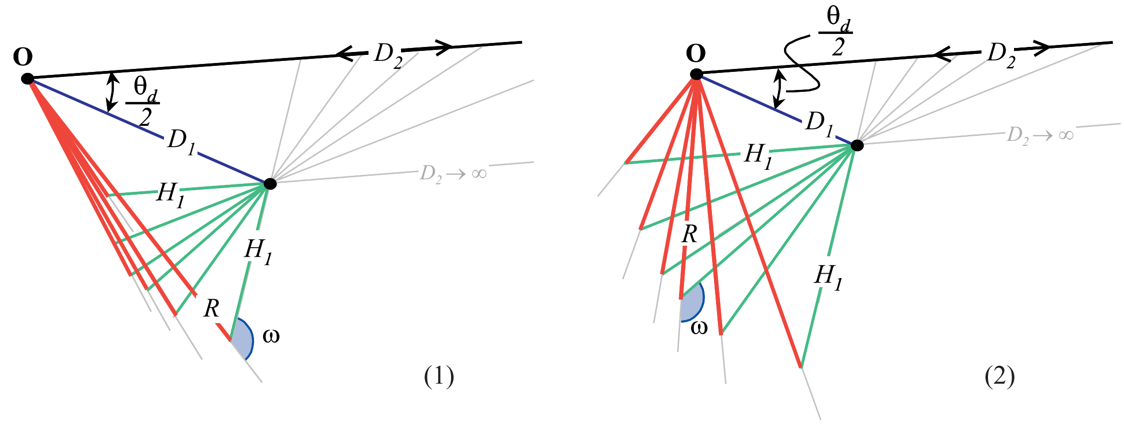

Figure 4: The geometry of changes in D_2 values and related changes of R and ω. In case (1) we have $D_1 \geq H_1$, and in case (2) we have $D_1 < H_1$.

From Fig. 3, we may observe that when the value of D_1 is increased from 0 to D_2, the value of R starts at R_-, decreases first and then increases again till it reaches its maximum R_+. There exists a minimum value of R, denoted as R_{min}. Let $D_1 = D_{1minR}$ when R reaches its minimum value, R_{min}. The values of D_{1minR} and R_{min} can be found by setting the first derivative equation of R equal to zero, and solving it with respect to D_1.

Similarly, from Fig. 3, we may also observe that when the value of D_1 is increased from 0 to D_2, the value of ω starts at ω_- (i.e. 180°), decreases first and then increases again till it reaches its maximum ω_+. There exist a minimum value of ω, denoted as ω_{min}. Let $D_1 = D_{1min\omega}$ when ω reaches its minimum value, ω_{min}. The values of $D_{1min\omega}$ and ω_{min} can be found by setting the first derivative equation of ω equal to zero, and solving it with respect to D_1.

Although the potential interval of D_1 is from 0 to D_2 exclusively, the valid interval of D_1 is smaller than the potential interval to ensure that the constraint $R < D_1$ holds. Since the functions of R and ω as shown in Eq. 3 and Eq. 4, are continuous over the potential interval of D_1, the valid interval of D_1 is an opened subinterval of $(0, D_2)$. The valid interval of D_1 is denoted as (D_{1-}, D_{1+}), and it contains the values of D_{1minR} and $D_{1min\omega}$.

3.2 How does a change of D_2 affect R and ω?

The value of D_2 is defined to be in the interval between D_1 and ∞ exclusively. The geometry of changes in D_2 versus changes in R and ω is depicted in Fig. 4. We separate the study into two cases: (1) $D_1 \geq H_1$, and (2) $D_1 < H_1$.

For both cases, when the value of D_2 goes to these two extreme values D_1 and ∞, the values of R are denoted as R_- and R_+ respectively. These can be written in limit notation as:

$$lim_{D_2 \to D_1^+} R = R_-, \text{ and } \lim_{D_2 \to \infty} R = R_+.$$

The value of R_- can be derived from Eq. 3, and is as follows:

$$R_- = \sqrt{D_1^2 + H_1^2 + 2D_1 H_1 \sin\left(\frac{\theta_r}{2}\right)}.$$

From Fig. 4, we observe that the value of R_+ is

$$R_+ = \sqrt{D_1^2 + H_1^2 - 2D_1 H_1 \cos(\theta_r)}.$$

Similarly for ω, we write

$$\lim_{D_2 \to D_1^+} \omega = \omega_-, \text{ and } \lim_{D_1 \to \infty} \omega = \omega_+.$$

The value of ω_- can be derived from Eq. 4, and is as follows:

$$\omega_- = \arccos\left(\frac{-H_1 - D_1 \sin\left(\frac{\theta_r}{2}\right)}{\sqrt{D_1^2 + H_1^2 + 2D_1 H_1 \sin\left(\frac{\theta_r}{2}\right)}}\right).$$

From Fig. 4, we observe that the value of ω_+ is

$$\omega_+ = 180^\circ - \arccos\left(\frac{H_1 - D_1 \cos(\theta_r)}{\sqrt{D_1^2 + H_1^2 - 2D_1 H_1 \cos(\theta_r)}}\right).$$

In both cases (1) and (2), we observe that $R_+ < R_-$ and the value of R decreases as the value of D_2 increases (i.e. the function R is decreasing monotonically on the interval D_2 in (D_1, ∞)). Thus, R_+ is the lower bound of R and R_- is the upper bound of R.

In case (1), when $D_1 \geq H_1$, we observe that $\omega_+ < \omega_-$ and the value of ω decreases as the value of D_2 increases (i.e. the function ω is decreasing monotonically on the interval D_2 in (D_1, ∞)). Thus, ω_+ is the lower bound of ω and ω_- is the upper bound of ω.

In case (2), when $D_1 < H_1$, we observe that when the value of D_2 is increased from D_1 to ∞, the value of ω starts at ω_-, decreases first and then increases again till it reaches its maximum ω_+. There exist a minimum value of ω, denoted as ω_{min}. Let $D_2 = D_{2min\omega}$ when ω reaches its minimum value, ω_{min}. The values of $D_{2min\omega}$ and ω_{min} can be found by letting the first derivative equation of ω equal to zero, and solving it with respect to D_2.

Although the potential interval of D_2 is from D_1 to ∞ exclusively, the valid interval of D_2 such that the constraint $R < D_1$ holds is smaller than the potential interval. Since the functions of R and ω as shown in Eq. 3 and Eq. 4 are continuous over the potential interval of D_2, the valid interval of D_2 is an opened subinterval of (D_1, ∞). The valid interval of D_2 is denoted as (D_{2-}, D_{2+}), and it contains the value $D_{2min\omega}$.

3.3 How does the change of H_1 affect R and ω?

Ideally, the value of H_1 can be any non-zero positive real number. The geometry of changing H_1 values versus changes in R and ω values is depicted in Fig. 5.

When the value of H_1 goes to its extremes, the corresponding values of R go to R_- and R_+, and can be written as

$$\lim_{H_1 \to 0^+} R = R_-, \text{ and } \lim_{H_1 \to \infty} R = R_+.$$

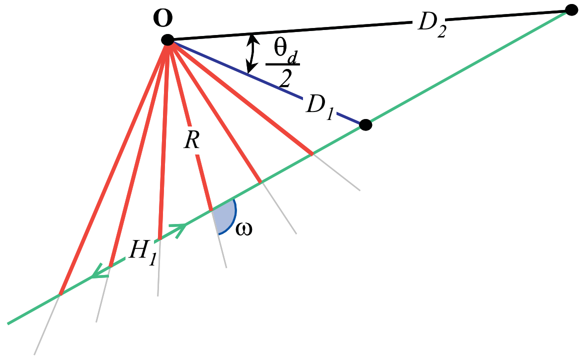

Figure 5: The geometry of changes in H_1 values and the related changes of R and ω.

From Eq. 3, it can easily be shown that $R_- = D_1$, and it is obvious that $R_+ = \infty$.

Similarly for ω, we write

$$\lim_{H_1 \to 0^+} \omega = \omega_-, \text{ and } \lim_{H_1 \to \infty} \omega = \omega_+.$$

From Eq. 4, it can easily be shown that $\omega_+ = 180°$, and the value of ω_- is as follows:

$$\omega_- = \arccos\left(\frac{D_2\cos(\theta_r) - D_1}{\sqrt{D_1^2 + D_2^2 - 2D_1D_2\cos(\theta_r)}}\right).$$

From Fig. 5, we may observe that when the value of H_1 is increased from 0 to ∞, the value of R starts at R_- (i.e. D_1), decreases first and then increases towards ∞. There exist a minimum value of R, denoted as R_{min}. Let $H_1 = H_{1minR}$ when R reaches to its minimum value, R_{min}. The values of H_{1minR} and R_{min} can be found by solving the first derivative equation of R (set it equal to zero) with respect to D_1.

$$H_{1minR} = \frac{D_1(D_1 - D_2\cos(\theta_r))}{\sqrt{D_1^2 + D_2^2 - 2D_1D_2\cos(\theta_r)}}.$$

From Fig. 5, we may also observe that the value of ω increases as the value of H_1 decreases (i.e. the function ω is increasing monotonically on the interval H_1 in $(0, \infty)$). Thus, ω_- is the lower bound of ω.

Although the potential interval of H_1 is from 0 to ∞ exclusively, the valid interval of H_1 such that the constraint $R < D_1$ holds is smaller than the potential interval. Since the functions of R and ω as shown in Eq. 3 and Eq. 4 are continuous over the potential interval of H_1, the valid interval of H_1 is an opened subinterval of $(0, \infty)$. The valid interval of H_1 is denoted as (H_{1-}, H_{1+}), and it contains the value of H_{1minR}. We have $H_{1-} = 0$ and

$$H_{1+} = \frac{2D_1(D_1 - D_2\cos(\theta_r))}{\sqrt{D_1^2 + D_2^2 - 2D_1D_2\cos(\theta_r)}}.$$

4 Error Analysis

The determination of R and ω requires values of d_r, f, u, D_1, D_2, and H_1. In this paper we only consider three independent errors introduced by independent measurements of D_1, D_2, and H_1. We are interested in observing how each of these measurement errors affects the application requirements, namely the possible scale of image disparities d_r and the camera-to-scene direction H_1, which influences the vertical field of view.

The errors of D_1, D_2, and H_1 are denoted as ε_{D_1}, ε_{D_2}, and ε_{H_1}, respectively. They are real numbers. The estimated values of D_1, D_2, and H_1 are denoted and defined as $\hat{D}_1 = D_1 + \varepsilon_{D_1}$, $\hat{D}_2 = D_2 + \varepsilon_{D_2}$, and $\hat{H}_1 = H_1 + \varepsilon_{H_1}$.

4.1 Parameter Dependency

In order to study how an error prorogates from an initial input value to the final resulting value, we must clarify the dependency among all the parameters. In this subsection, we list algebraic dependencies following the steps of an acquisition procedure. The notation $Y = f_Y(X_1, X_2, \ldots, X_n)$ means that parameter Y depends on parameters $X_1, X_2, \ldots, X_n$. In other words, parameter Y is a function of variables $X_1, X_2, \ldots, X_n$.

The number of slit images taken for a 360° view (i.e. the number of image columns W_P) is calculated based on values of f, u, D_1, and H_1, which is shown in Eq. 1. We write $W_P = f_{W_P}(f, u, D_1, H_1)$. The angular disparity width θ_r is determined by the image disparity width d_r and the number of image columns W_P, as shown in Eq. 2: we have $\theta_r = f_{\theta_r}(d_r, W_P)$.

A suitable value of R for image acquisition is determined according to the values of D_1, D_2, H_1, and θ_r, which is shown in Eq. 3. Thus, we have $R = f_R(D_1, D_2, H_1, \theta_r)$. The camera viewing angle ω is determined also according to the values of D_1, D_2, H_1, and θ_r, which is shown in Eq. 4. Hence, we have $\omega = f_\omega(D_1, D_2, H_1, \theta_r)$.

Now consider a case where values of R and ω are used for image acquisition as calculated by our formulas in Eq. 3 and Eq. 4. Exactly these values are assumed to set up a camera and to capture images in a real 3D scene with a RoI represented by D_1 and D_2. We may backtrack the values of H_1 and θ_r according to the values of R, ω, D_1 and D_2. The value of H_1 can be calculated by the following formula:

$$H_1 = \sqrt{D_1^2 + R^2\cos(2\alpha) + 2R\cos(\alpha)\sqrt{D_1^2 - R^2\sin^2(\alpha)}}, \tag{6}$$

where $\alpha = (180° - \omega)$. So, we may write $H_1 = f_{H_1}(D_1, R, \omega)$. The value of θ_r can be calculated by the following formula:

$$\theta_r = \arcsin\left(\frac{R}{D_1 D_2}\sin(\omega)\left(\sqrt{D_2^2 - R^2\sin^2(\omega)} - \sqrt{D_1^2 - R^2\sin^2(\omega)}\right)\right), \tag{7}$$

Thus, we have $\theta_r = f_{\theta_r}(D_1, D_2, R, \omega)$. Assuming an error free process, then the values H_1 and θ_r calculated here (after image acquisition) should be identical to the originally stated requirements.

Furthermore, the image disparity width can be obtained from the values of θ_r and W_P. So, finally we have $d_r = f_{d_r}(\theta_r, W_P)$.

4.2 Error of D_1

The calculation of the number of image columns depends on D_1. If the value of $\hat{D}_1$ contains an error (i.e. $|\varepsilon_{D_1}| > 0$), then we obtain an incorrect value of W_P, denoted as $\hat{W}_P$. Using this value of $\hat{W}_P$ to calculate θ_r we obtain an incorrect value of θ_r denoted as $\hat{\theta}_r$.

Both functions of R and ω in Eqs. 3 and 4 are functions of four variables D_1, D_2, H_1 and θ_r. So, if the values of $\hat{W}_P$ and $\hat{\theta}_r$ contain errors, then the determined values of R and ω also contain errors. The errors of R and ω are denoted as ε_R and ε_ω respectively and they are defined as

$$\begin{aligned}\varepsilon_R &= \hat{R} - R,\\ &= f_R(\hat{D}_1, D_2, H_1, \hat{\theta}_r) - f_R(D_1, D_2, H_1, \theta_r)\end{aligned}$$

and

$$\begin{aligned}\varepsilon_\omega &= \hat{\omega} - \omega,\\ &= f_\omega(\hat{D}_1, D_2, H_1, \hat{\theta}_r) - f_\omega(D_1, D_2, H_1, \theta_r).\end{aligned}$$

	D_1	D_2	H_1	W_P	θ_d	R	ω
(1)	1	5	1.2	16232	10.48	0.2359	151.10
(2)	4	20	4.2	18550	9.17	0.4555	118.87
(3)	6	50	5.5	21249	8.00	0.6768	44.66
(4)	20	200	20.0	19478	8.74	1.6942	92.43

H_P = 5184 (pixels) u = 0.007 (mm)
H_S = 768 (pixels) f = 21.7 (mm)

Table 1: Four practical examples: (1) close-range indoor, (2) far-range indoor, (3) close-range outdoor, and (4) far-range outdoor scenes.

We define four examples in Tab. 1. The numerical relationships between errors of D_1 and errors of R and ω is documented in Tab. 2 for these four examples. All the errors are measured in percentage. The error interval of D_1 is in $[-10\%, +10\%]$.

When the error of D_1 is increasing from -10% to $+10\%$, the error of R in our four examples has different changing behavior. Let us observe how ε_R changes in each example according to the studies in Sec. 3. In fact the $\pm 10\%$ error interval of D_1 may be considered to be a very small interval of the interval of possible D_1 values. For example, in case (1), when ε_{D_1} changes from -10% to $+10\%$, ε_R changes from 38.37%, decreasing monotonically, to -33.02%, which means the interval of a $\pm 10\%$ error of D_1 does not contain the value D_{1minR} (i.e. when R reaches its minimum). In the example (4), ε_R changes from 57.57%, decreasing and reaching a minimum when $\varepsilon_{D_1} = 0$, then increases again, to 52.49%, which means the value D_{1minR} roughly lies at the center of the error interval of D_1.

When the error of D_1 is increasing from -10% to $+10\%$, the errors of ω in our four examples decrease monotonically, which means that the error interval of D_1 dose not contain the value $D_{1min\omega}$. This is because the value of $D_{1min\omega}$ is very small in most cases.

The values of $\hat{R}$ and $\hat{\omega}$ are used to calculate H_1 and θ_r using the equations shown in Eqs. 6 and 7. We obtain values $\hat{H}_1$ and $\hat{\hat{\theta}}_r$, and both contain errors. Finally, the image disparity width can be obtained, denoted as $\hat{d}_r$, which also contains an error. The errors introduced in the obtained $\hat{H}_1$ and $\hat{d}_r$ values are denoted as ε_{H_1} and ε_{d_r} respectively.

The relations between ε_{D_1} and ε_{H_1} and ε_{d_r} (for our four examples) are numerically documented in Tab. 2 and graphically in Fig. 6. The relations between these errors are approximately linear, and the quantities are relatively close. Note that although the error of D_1 does have significant impact on the estimated values of $\hat{R}$ and $\hat{\omega}$, the resulting values of $\hat{H}_1$ and $\hat{d}_r$ have only $\approx \pm 10\%$ error, which might be acceptable for some applications.

$\frac{\varepsilon_{D_1}}{D_1}$ (%)	$\hat{D}_1$	$\hat{R}$	$\frac{\varepsilon_R}{R}$ (%)	$\hat{\omega}$	$\frac{\varepsilon_\omega}{\omega}$ (%)	$\hat{d}$	$\frac{\varepsilon_d}{d}$ (%)	$\hat{H}_1$	$\frac{\varepsilon_{H_1}}{H_1}$ (%)
-10	0.90	0.3264	38.37	160.08	5.95	61.4	-12.24	1.3007	8.39
-8	0.92	0.3078	30.49	158.71	5.04	63.1	-9.84	1.2805	6.71
-6	0.94	0.2894	22.69	157.17	4.02	64.8	-7.42	1.2604	5.03
-4	0.96	0.2712	14.99	155.41	2.86	66.5	-4.97	1.2402	3.36
-2	0.98	0.2534	7.42	153.40	1.53	68.3	-2.50	1.2201	1.68
0	1.00	0.2359	0.00	151.10	0.00	70.0	0.00	1.2000	0.00
2	1.02	0.2188	-7.23	148.42	-1.77	71.8	2.52	1.1798	-1.68
4	1.04	0.2023	-14.22	145.31	-3.83	73.5	5.07	1.1597	-3.35
6	1.06	0.1866	-20.90	141.65	-6.25	75.4	7.64	1.1396	-5.03
8	1.08	0.1717	-27.21	137.33	-9.11	77.2	10.24	1.1195	-6.71
10	1.10	0.1580	-33.02	132.24	-12.48	79.0	12.87	1.0993	-8.39

Example (1)

$\frac{\varepsilon_{D_1}}{D_1}$ (%)	$\hat{D}_1$	$\hat{R}$	$\frac{\varepsilon_R}{R}$ (%)	$\hat{\omega}$	$\frac{\varepsilon_\omega}{\omega}$ (%)	$\hat{d}$	$\frac{\varepsilon_d}{d}$ (%)	$\hat{H}_1$	$\frac{\varepsilon_{H_1}}{H_1}$ (%)
-10	3.60	0.7332	60.83	147.92	24.44	61.4	-12.23	4.6023	9.57
-8	3.68	0.6677	46.45	144.12	21.24	63.1	-9.83	4.5218	7.66
-6	3.76	0.6058	32.87	139.51	17.37	64.8	-7.41	4.4414	5.74
-4	3.84	0.5487	20.34	133.91	12.66	66.5	-4.97	4.3609	3.83
-2	3.92	0.4980	9.23	127.09	6.92	68.3	-2.50	4.2805	1.91
0	4.00	0.4559	0.00	118.87	0.00	70.0	0.00	4.2000	0.00
2	4.08	0.4250	-6.78	109.22	-8.11	71.8	2.52	4.1197	-1.91
4	4.16	0.4078	-10.57	98.42	-17.20	73.5	5.07	4.0393	-3.83
6	4.24	0.4059	-10.97	87.11	-26.71	75.3	7.64	3.9590	-5.74
8	4.32	0.4197	-7.94	76.13	-35.95	77.2	10.23	3.8786	-7.66
10	4.40	0.4477	-1.80	66.19	-44.32	79.0	12.86	3.7982	-9.57

Example (2)

$\frac{\varepsilon_{D_1}}{D_1}$ (%)	$\hat{D}_1$	$\hat{R}$	$\frac{\varepsilon_R}{R}$ (%)	$\hat{\omega}$	$\frac{\varepsilon_\omega}{\omega}$ (%)	$\hat{d}$	$\frac{\varepsilon_d}{d}$ (%)	$\hat{H}_1$	$\frac{\varepsilon_{H_1}}{H_1}$ (%)
-10	5.40	0.4844	-28.43	104.37	133.68	62.1	-11.23	6.1018	10.95
-8	5.52	0.4705	-30.48	89.98	101.47	63.7	-9.01	5.9814	8.76
-6	5.64	0.4869	-28.05	75.68	69.44	65.3	-6.78	5.8610	6.57
-4	5.76	0.5308	-21.56	63.03	41.12	66.8	-4.53	5.7405	4.38
-2	5.88	0.5962	-11.91	52.73	18.05	68.4	-2.27	5.6202	2.19
0	6.00	0.6768	0.00	44.66	0.00	70.0	0.00	5.5000	0.00
2	6.12	0.7678	13.45	38.41	-14.00	71.6	2.28	5.3794	-2.19
4	6.24	0.8660	27.96	33.53	-24.82	73.2	4.58	5.2590	-4.38
6	6.36	0.9692	43.21	29.67	-33.58	74.8	6.89	5.1387	-6.57
8	6.48	1.0759	58.98	26.56	-40.54	76.4	9.21	5.0183	-8.75
10	6.60	1.1852	75.13	24.02	-46.23	78.1	11.54	4.8980	-10.94

Example (3)

$\frac{\varepsilon_{D_1}}{D_1}$ (%)	$\hat{D}_1$	$\hat{R}$	$\frac{\varepsilon_R}{R}$ (%)	$\hat{\omega}$	$\frac{\varepsilon_\omega}{\omega}$ (%)	$\hat{d}$	$\frac{\varepsilon_d}{d}$ (%)	$\hat{H}_1$	$\frac{\varepsilon_{H_1}}{H_1}$ (%)
-10	18.0	2.6674	57.57	141.17	52.73	62.3	-11.01	22.008	10.04
-8	18.4	2.3708	40.05	135.01	46.06	63.8	-8.83	21.606	8.03
-6	18.8	2.1092	24.59	127.21	37.62	65.4	-6.64	21.205	6.02
-4	19.2	1.8971	12.07	117.44	27.05	66.9	-4.43	20.803	4.01
-2	19.6	1.7525	3.53	105.66	14.31	68.4	-2.22	20.402	2.01
0	20.0	1.6928	0.00	92.43	0.00	70.0	0.00	20.000	0.00
2	20.4	1.7268	2.01	79.01	-14.52	71.6	2.23	19.600	-2.01
4	20.8	1.8493	9.24	66.74	-27.80	73.1	4.47	19.197	-4.01
6	21.2	2.0444	20.77	56.40	-38.98	74.7	6.73	18.796	-6.02
8	21.6	2.2937	35.49	48.08	-47.98	76.3	8.99	18.395	-8.03
10	22.0	2.5814	52.49	41.51	-55.10	77.9	11.26	17.994	-10.03

Example (4)

Table 2: The propagation of errors of D_1 to $\hat{H}_1$ and $\hat{d}_r$.

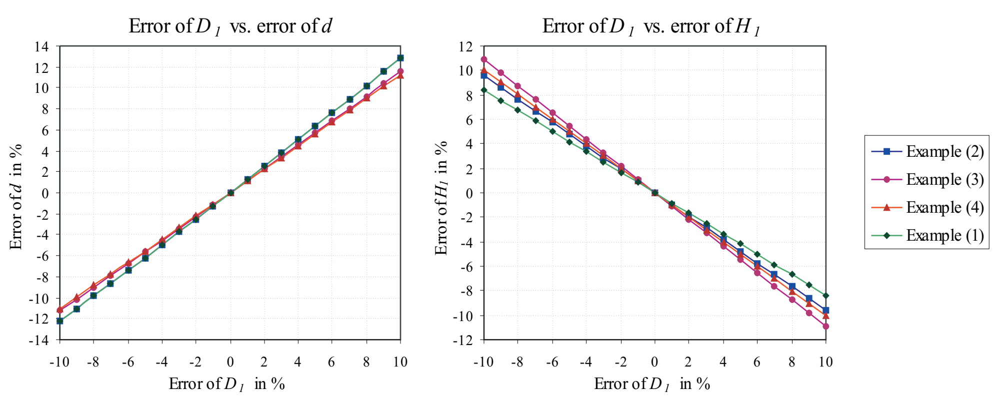

Figure 6: The errors of D_1 vs. errors of H_1 and d_r.

4.3 Error of D_2

If the value of the estimated $\hat{D}_1$ contains an error (i.e. $|\varepsilon_{D_1}| > 0$), then we obtain an incorrect value of R and ω, denoted as $\hat{R}$ and $\hat{\omega}$. The errors of R and ω are denoted as ε_R and ε_ω respectively and they are defined as

$$\begin{aligned}\varepsilon_R &= \hat{R} - R, \\ &= f_R(D_1, \hat{D}_2, H_1, \theta_r) - f_R(D_1, D_2, H_1, \theta_r)\end{aligned}$$

and

$$\begin{aligned}\varepsilon_\omega &= \hat{\omega} - \omega, \\ &= f_\omega(D_1, \hat{D}_2, H_1, \theta_r) - f_\omega(D_1, D_2, H_1, \theta_r).\end{aligned}$$

We refer again to our four examples defined in Tab. 2. An error in D_2 produces errors in R and ω which are shown in Tab. 3 in percentage. The error interval of D_2 is in $[-10\%, +10\%]$.

When the error of D_2 is increasing from -10% to $+10\%$, the error of R decreases monotonically in our four examples. This is because R is decreasing monotonically on the valid interval of D_2, as stated in Sec. 3.2. The quantity of the error of R introduced by ε_{D_2} is much smaller in comparison to ε_{D_1}. In particular for the examples (1) and (2), both belonging to the case of $D_1 < H_1$, when the error of D_2 is increased from -10% to $+10\%$, the error of ω decrease monotonically and the error interval of D_2 dose not contain the value $D_{2min\omega}$ for both examples.

Since the values of $\hat{R}$ and $\hat{\omega}$ are used to calculate H_1 and θ_r, using Eqs. 6 and 7 we have $\hat{H}_1$ and $\hat{\theta}_r$. Similarly, the image disparity width can be obtained and denoted as $\hat{d}_r$.

The errors introduced in the obtained $\hat{H}_1$ and $\hat{d}_r$ are denoted as ε_{H_1} and ε_{d_r} respectively. The relation between ε_{D_1} and each of ε_{H_1} and ε_{d_r} is shown in Tab. 3. We obtain that $\varepsilon_{H_1} = 0$, which means

$$\hat{H}_1 = f_{H_1}(D_1, \hat{R}, \hat{\omega}) = H_1.$$

This suggests ε_{D_2} has no impact on H_1. Figure 7 shows the plot of $\hat{D}_2$ vs. ε_{d_r}.

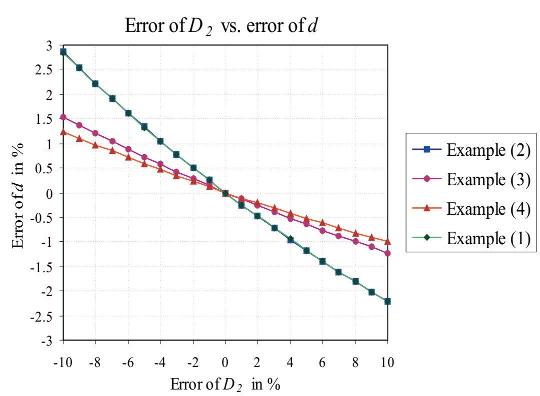

Figure 7: The errors of D_2 vs. error of d_r.

$\frac{\varepsilon_{D_2}}{D_2}$ (%)	$\hat{D}_2$	$\hat{R}$	$\frac{\varepsilon_R}{R}$ (%)	$\hat{\omega}$	$\frac{\varepsilon_\omega}{\omega}$ (%)	$\hat{d}$	$\frac{\varepsilon_d}{d}$ (%)	$\hat{H}_1$	$\frac{\varepsilon_{H_1}}{H_1}$ (%)
-10	4.50	0.2378	0.81	150.46	-0.42	72.0	2.85	1.2000	0.00
-8	4.60	0.2373	0.63	150.60	-0.33	71.6	2.22	1.2000	0.00
-6	4.70	0.2369	0.46	150.73	-0.24	71.1	1.62	1.2000	0.00
-4	4.80	0.2366	0.30	150.86	-0.16	70.7	1.05	1.2000	0.00
-2	4.90	0.2362	0.14	150.98	-0.08	70.4	0.51	1.2000	0.00
0	5.00	0.2359	0.00	151.10	0.00	70.0	0.00	1.2000	0.00
2	5.10	0.2355	-0.14	151.21	0.07	69.7	-0.49	1.2000	0.00
4	5.20	0.2352	-0.27	151.31	0.14	69.3	-0.95	1.2000	0.00
6	5.30	0.2349	-0.39	151.41	0.21	69.0	-1.39	1.2000	0.00
8	5.40	0.2347	-0.51	151.51	0.27	68.7	-1.81	1.2000	0.00
10	5.50	0.2344	-0.62	151.60	0.33	68.4	-2.22	1.2000	0.00

Example (1)

$\frac{\varepsilon_{D_2}}{D_2}$ (%)	$\hat{D}_2$	$\hat{R}$	$\frac{\varepsilon_R}{R}$ (%)	$\hat{\omega}$	$\frac{\varepsilon_\omega}{\omega}$ (%)	$\hat{d}$	$\frac{\varepsilon_d}{d}$ (%)	$\hat{H}_1$	$\frac{\varepsilon_{H_1}}{H_1}$ (%)
-10	18.0	0.4664	2.30	118.32	-0.46	72.0	2.85	4.2000	0.00
-8	18.4	0.4641	1.79	118.44	-0.36	71.6	2.22	4.2000	0.00
-6	18.8	0.4619	1.31	118.55	-0.26	71.1	1.62	4.2000	0.00
-4	19.2	0.4598	0.85	118.66	-0.17	70.7	1.05	4.2000	0.00
-2	19.6	0.4578	0.41	118.77	-0.08	70.4	0.51	4.2000	0.00
0	20.0	0.4559	0.00	118.87	0.00	70.0	0.00	4.2000	0.00
2	20.4	0.4541	-0.39	118.96	0.08	69.7	-0.49	4.2000	0.00
4	20.8	0.4524	-0.77	119.06	0.16	69.3	-0.95	4.2000	0.00
6	21.2	0.4508	-1.12	119.14	0.23	69.0	-1.39	4.2000	0.00
8	21.6	0.4493	-1.46	119.23	0.31	68.7	-1.81	4.2000	0.00
10	22.0	0.4478	-1.78	119.31	0.38	68.4	-2.22	4.2000	0.00

Example (2)

$\frac{\varepsilon_{D_2}}{D_2}$ (%)	$\hat{D}_2$	$\hat{R}$	$\frac{\varepsilon_R}{R}$ (%)	$\hat{\omega}$	$\frac{\varepsilon_\omega}{\omega}$ (%)	$\hat{d}$	$\frac{\varepsilon_d}{d}$ (%)	$\hat{H}_1$	$\frac{\varepsilon_{H_1}}{H_1}$ (%)
-10	45.0	0.6815	0.70	45.13	1.05	71.1	1.54	5.5000	0.00
-8	46.0	0.6804	0.55	45.03	0.82	70.8	1.20	5.5000	0.00
-6	47.0	0.6795	0.40	44.93	0.60	70.6	0.88	5.5000	0.00
-4	48.0	0.6785	0.26	44.84	0.39	70.4	0.57	5.5000	0.00
-2	49.0	0.6776	0.13	44.75	0.19	70.2	0.28	5.5000	0.00
0	50.0	0.6768	0.00	44.66	0.00	70.0	0.00	5.5000	0.00
2	51.0	0.6759	-0.12	44.58	-0.18	69.8	-0.27	5.5000	0.00
4	52.0	0.6752	-0.24	44.50	-0.36	69.6	-0.52	5.5000	0.00
6	53.0	0.6744	-0.35	44.43	-0.53	69.5	-0.77	5.5000	0.00
8	54.0	0.6737	-0.45	44.35	-0.69	69.3	-1.00	5.5000	0.00
10	55.0	0.6730	-0.55	44.28	-0.85	69.1	-1.22	5.5000	0.00

Example (3)

$\frac{\varepsilon_{D_2}}{D_2}$ (%)	$\hat{D}_2$	$\hat{R}$	$\frac{\varepsilon_R}{R}$ (%)	$\hat{\omega}$	$\frac{\varepsilon_\omega}{\omega}$ (%)	$\hat{d}$	$\frac{\varepsilon_d}{d}$ (%)	$\hat{H}_1$	$\frac{\varepsilon_{H_1}}{H_1}$ (%)
-10	180.0	2.6674	1.25	92.46	0.03	70.9	1.25	20.000	0.00
-8	184.0	2.3708	0.97	92.46	0.03	70.7	0.97	20.000	0.00
-6	188.0	2.1092	0.71	92.45	0.02	70.5	0.71	20.000	0.00
-4	192.0	1.8971	0.46	92.44	0.01	70.3	0.46	20.000	0.00
-2	196.0	1.7525	0.23	92.44	0.01	70.2	0.23	20.000	0.00
0	200.0	1.6928	0.00	92.43	0.00	70.0	0.00	20.000	0.00
2	204.0	1.7268	-0.22	92.43	-0.01	69.8	-0.22	20.000	0.00
4	208.0	1.8493	-0.42	92.42	-0.01	69.7	-0.42	20.000	0.00
6	212.0	2.0444	-0.62	92.42	-0.02	69.6	-0.62	20.000	0.00
8	216.0	2.2937	-0.81	92.41	-0.02	69.4	-0.82	20.000	0.00
10	220.0	2.5814	-1.00	92.41	-0.03	69.3	-1.00	20.000	0.00

Example (4)

Table 3: The propagation of errors of D_2 to $\hat{H}_1$ and $\hat{d}_r$.

4.4 Error of H_1

If the absolute value of the error of H_1 is greater than zero (i.e. $|\varepsilon_{H_1}| > 0$), then we obtain an incorrect value of W_P, denoted as $\hat{W}_P$, because the calculation of the number of image columns depends on D_1. Then, using the value of $\hat{W}_P$ we obtain $\hat{\theta}_r$.

Both functions for R and ω in Eqs. 3 and 4 are functions of four variables D_1, D_2, H_1 and θ_r. So, if the estimated values of $\hat{W}_P$ and $\hat{\theta}_r$ contain errors, then the determined values of R and ω also contain errors. The errors of R and ω are denoted as ε_R and ε_ω respectively and they are defined as

$$\begin{aligned} \varepsilon_R &= \hat{R} - R, \\ &= f_R(D_1, D_2, \hat{H}_1, \hat{\theta}_r) - f_R(D_1, D_2, H_1, \theta_r) \end{aligned}$$

and

$$\begin{aligned} \varepsilon_\omega &= \hat{\omega} - \omega, \\ &= f_\omega(D_1, D_2, \hat{H}_1, \hat{\theta}_r) - f_\omega(D_1, D_2, H_1, \theta_r). \end{aligned}$$

We refer to our four acquisition examples again to show the relation between the error of H_1 and the errors of R and ω see Tab. 4. The error interval of H_1 is in $[-10\%, +10\%]$. The values of $\hat{R}$ and $\hat{\omega}$ are used to calculate θ_r using the equation shown in Eq. 7. We obtain the previous value of $\hat{\theta}_r$. Hence, there is no error in the obtained d_r value.

$\frac{\varepsilon_{H_1}}{H_1}$ (%)	$\hat{H}_1$	$\hat{R}$	$\frac{\varepsilon_R}{R}$ (%)	$\hat{\omega}$	$\frac{\varepsilon_\omega}{\omega}$ (%)	$\hat{d}$	$\frac{\varepsilon_d}{d}$ (%)
-10	1.080	0.1334	-43.43	129.71	-14.16	70.0	0.00
-8	1.104	0.1516	-35.71	136.22	-9.85	70.0	0.00
-6	1.128	0.1714	-27.34	141.28	-6.49	70.0	0.00
-4	1.152	0.1922	-18.51	145.28	-3.85	70.0	0.00
-2	1.176	0.2138	-9.37	148.48	-1.73	70.0	0.00
0	1.200	0.2359	0.00	151.10	0.00	70.0	0.00
2	1.224	0.2584	9.55	153.26	1.43	70.0	0.00
4	1.248	0.2812	19.23	155.07	2.63	70.0	0.00
6	1.272	0.3043	29.01	156.61	3.65	70.0	0.00
8	1.296	0.3276	38.88	157.93	4.52	70.0	0.00
10	1.320	0.3510	48.81	159.08	5.28	70.0	0.00

Example (1)

$\frac{\varepsilon_{H_1}}{H_1}$ (%)	$\hat{H}_1$	$\hat{R}$	$\frac{\varepsilon_R}{R}$ (%)	$\hat{\omega}$	$\frac{\varepsilon_\omega}{\omega}$ (%)	$\hat{d}$	$\frac{\varepsilon_d}{d}$ (%)
-10	3.78	0.4132	-9.37	60.46	-49.13	70.0	0.00
-8	3.86	0.3862	-15.29	72.06	-39.38	70.0	0.00
-6	3.95	0.3770	-17.32	84.79	-28.67	70.0	0.00
-4	4.03	0.3867	-15.19	97.51	-17.97	70.0	0.00
-2	4.12	0.4141	-9.18	109.07	-8.24	70.0	0.00
0	4.2	0.4559	0.00	118.87	0.00	70.0	0.00
2	4.28	0.5087	11.58	126.82	6.69	70.0	0.00
4	4.37	0.5695	24.90	133.19	12.05	70.0	0.00
6	4.45	0.6358	39.45	138.28	16.33	70.0	0.00
8	4.54	0.7063	54.90	142.38	19.78	70.0	0.00
10	4.62	0.7797	71.00	145.73	22.60	70.0	0.00

Example (2)

$\frac{\varepsilon_{H_1}}{H_1}$ (%)	$\hat{H}_1$	$\hat{R}$	$\frac{\varepsilon_R}{R}$ (%)	$\hat{\omega}$	$\frac{\varepsilon_\omega}{\omega}$ (%)	$\hat{d}$	$\frac{\varepsilon_d}{d}$ (%)
-10	4.95	1.1200	65.50	22.48	-49.67	70.0	0.00
-8	5.06	1.0226	51.11	25.34	-43.26	70.0	0.00
-6	5.17	0.9284	37.18	28.8	-35.52	70.0	0.00
-4	5.28	0.8382	23.85	33.02	-26.07	70.0	0.00
-2	5.39	0.7536	11.36	38.22	-14.43	70.0	0.00
0	5.5	0.6768	0.00	44.66	0.00	70.0	0.00
2	5.61	0.6105	-9.78	52.63	17.83	70.0	0.00
4	5.72	0.5588	-17.43	62.29	39.47	70.0	0.00
6	5.83	0.5258	-22.31	73.53	64.64	70.0	0.00
8	5.94	0.5151	-23.89	85.74	91.98	70.0	0.00
10	6.05	0.5282	-21.95	97.9	119.19	70.0	0.00

Example (3)

$\frac{\varepsilon_{H_1}}{H_1}$ (%)	$\hat{H}_1$	$\hat{R}$	$\frac{\varepsilon_R}{R}$ (%)	$\hat{\omega}$	$\frac{\varepsilon_\omega}{\omega}$ (%)	$\hat{d}$	$\frac{\varepsilon_d}{d}$ (%)
-10	180.0	2.6674	1.25	92.46	0.03	70.0	0.00
-8	184.0	2.3708	0.97	92.46	0.03	70.0	0.00
-6	188.0	2.1092	0.71	92.45	0.02	70.0	0.00
-4	192.0	1.8971	0.46	92.44	0.01	70.0	0.00
-2	196.0	1.7525	0.23	92.44	0.01	70.0	0.00
0	200.0	1.6928	0.00	92.43	0.00	70.0	0.00
2	204.0	1.7268	-0.22	92.43	-0.01	70.0	0.00
4	208.0	1.8493	-0.42	92.42	-0.01	70.0	0.00
6	212.0	2.0444	-0.62	92.42	-0.02	70.0	0.00
8	216.0	2.2937	-0.81	92.41	-0.02	70.0	0.00
10	220.0	2.5814	-1.00	92.41	-0.03	70.0	0.00

Example (4)

Table 4: The propagation of errors of H_1 to $\hat{H}_1$ and $\hat{d}_r$.

5 Conclusions and Future Work

This paper defined a new approach towards the study of basic algebraic relations between application requirements, image acquisition models, and specifications of a RoI in 3D scenes. The paper analyzed how application-specific parameters affect the imaging parameters, and what are possible intervals of values of these parameters. We also discussed error propagation, from the measurements of application-specific parameters to the imaging parameters and finally to the application-requirement parameters. These propagations are explored and described for various practical examples.

Although ε_{D_1} affects R and ω quadratically, the impacts to d_r and H_1 are approximately linear. Similar statements can be made for for ε_{D_2} and ε_{H_1}, however, ε_{D_1} has stronger influence in terms of magnitude. Interestingly, ε_{D_2} has no impact on H_1 and ε_{H_1} has no impact on d_r.

In future work, we will answer the following questions: Which R value and what interval of ωshould be chosen to built a camera for given intervals of D_1 D_2 H_1 and θ_r which are defined by an application? Furthermore, specifying possible intervals for R and ω, what intervals of D_1 D_2 H_1 and θ_r can be ensured by a panoramic imaging system?

Acknowledgments

The first author thanks the space sensory institute of DLR (German Aerospace Center) for an efficient research visit in March 2001 allowing a further specification of our panoramic camera model in accordance with recent line camera technologies.

References

[Che95] S. E. Chen. QuickTimeVR - an image-based approach to virtual environment navigation. In *Proc. SIGGRAPH'95*, pages 29–38, Los Angeles, California, USA, August 1995.

[HWK01] F. Huang, S. K. Wei, and R. Klette. Geometrical fundamentals of polycentric panoramas. In *Proc. ICCV01*, pages 560–565, Vancouver, Canada, July 2001.

[IYT92] H. Ishiguro, M. Yamamoto, and S. Tsuji. Omni-directional stereo. *PAMI*, 14(2):257–262, 1992.

[PBE99] S. Peleg and M. Ben-Ezra. Stereo panorama with a single camera. In *Proc. CVPR99*, pages 395–401, Fort Collins, Colorado, USA, June 1999.

[RS97] R. Reulke and M. Scheel. Ccd-line digital imager for photogrammetry in architecture. *nt. Archives of Photogrammetry and Remote Sensing*, XXXII(5C18):195–201, 1997.

[Sei01] S. M. Seitz. The space of all stereo images. In *Proc. ICCV01*, pages 26–33, Vancouver, Canada, July 2001.

[SH99] H.-Y. Shum and L.-W. He. Rendering with concentric mosaics. In *Proc. SIGGRAPH'99*, pages 299–306, Los Angeles, California, USA, August 1999.

[SKS99] H. Shum, A. Kalai, and S. Seitz. Omnivergent stereo. In *Proc. ICCV99*, pages 22–29, Korfu, Greece, September 1999.

[SS97] R. Szeliski and H.-Y. Shum. Creating full view panoramic image mosaics and environment maps. In *Proc. SIGGRAPH'97*, pages 251–258, Los Angeles, California, USA, August 1997.

[WHK99] S.-K. Wei, F. Huang, and R. Klette. Three-dimensional scene navigation through anaglyphic panorama visualization. In *Proc. CAIP99*, pages 542–549, Ljubljana, Slovenia, September 1999.

[WHK00] S.-K. Wei, F. Huang, and R. Klette. Classification and characterization of image acquisition for 3d scene visualization and reconstruction applications. In *Multi-image analysis*, pages xx–yy, Dagstuhl, Germany, March 2000.